This is a peer-reviewed, accepted author manuscript of the following research article: Hopper, C., Pruncu, C., Hooper, P. A., Tan, Z., Yang, S-T., Liu, Y., & Jiang, J. (Accepted/In press). The effects of hot forging on the preform additive manufactured 316 stainless steel parts. *Micron*, [103026].

The effects of hot forging on the preform additive manufactured 316 stainless steel parts

Christopher Hopper[a], Catalin I. Pruncu[a,b*], Paul A. Hooper[a], Zinong Tan[a], Shang-Te Yang, Yuehan Liu[a], Jun Jiang[a]

[a]Department of Mechanical Engineering, Imperial College London, Exhibition Road, SW7 2AZ, London, UK.
[b]Design, Manufacturing & Engineering Management, University of Strathclyde, Glasgow, G1 1XJ, Scotland, UK
corresponding author: c.pruncu@imperial.ac.uk

Abstract

Additive Manufacture (AM) offers great potential for creating metallic parts for high end products used in critical application i.e. aerospace and biomedical engineering. General acceptance of AM within these fields has been held back by a lack of confidence in the consistency of the mechanical properties of AMed parts associated by the occurrence of porosity, large columnar grains and texture. In this research, to counters this problem we have combined hot forging and subsequent heat treatment. Although, perhaps not best suited to components featuring fine detail, this technique should be well suited to the manufacture of forged components such as fan blades. Here, AM is able to create a near net-shape blank which is then hot forged to size, eliminating intermediate production stages and generating good mechanical properties in the final component. The material used in the current study is AM 316L Stainless Steel. By altering the printing parameters of the AM machine, two batches of samples were built, each displaying a different porosity content. This allowed the influence of initial build quality to be illustrated. By comparing the two sample batches, it was possible to gain an insight into the possibilities of controlling porosity and material microstructure. The success of the proposed hot forging and heat treatment technique was validated by mechanical testing (i.e. tensile and hardness experiments) and microstructure evolution characterization (i.e. optical microscopy observation and electron backscatter diffraction (EBSD) techniques). The results revealed that the post processing strategy reduced material porosity and enabled the creation of a more robust microstructure, resulting in improved mechanical properties of the AM material.

Key words: 316L stainless steel, Additive Manufacturing (AM), Electron Back Scatter Diffraction (EBSD) grain recrystallization, forging and heat treatment.

1. Introduction

The research presented here investigates the use of hot forging as a technique for improving the mechanical properties and industrial application of metallic AM components. Over the last two decades, the AM process has emerged as one of the most significant drivers in commercial metallic material manufacturing technologies, as described by Frazier [1]. Automotive, aerospace, and healthcare industries encouraged the use of AM in their businesses because of great advantages. According to Kruth et al. [2], the use of AM for rapid prototyping can generate significant economic and technological development. AM technology is defined as a process of fusing materials together layer by layer and finally forming a 3D model from CAD data. Its emergence is related to the great potential for manufacturing complex geometry that are difficult or impossible to manufacture by conventional machining or casting operations [3]. Ghouse et al. [4] found that by using AM methods such as Powder Bed Fusion (PBF) they were able to manufacture parts with abstract shapes within short lead-times and with no tooling costs. Despite these great potential advantages, the reality of moving the AM into large

scale production is restricted by robust control of manufacturing parameters, which can lead to the manufacture of parts with defined microstructures and minimal defects.

Lee et al. [5] highlighted that the properties of AM materials produced by laser PBF depend on a larger number of process parameters such as average laser power, power stability, central wavelength, spectral bandwidth, beam diameter, beam quality, pulse energy, pulse duration, repetition rate, the build orientation/direction and the tool path. Indeed, Wang et al. [6] and Pellizzari et al. [7] produced superior AM parts by varying the deposition strategies. Further, as indicated by Karimi et al. [8], it is expected that when the laser exposure time is increased, combined with decreasing hatch spacing both the presence of gas porosity and the lack of fusion will reduce. Cherry et al. [9] revealed that by varying the laser energy density it is possible to produce dense parts with minimum porosity. Another study conducted by Pragana et al. [10] revealed that the manufacturing environment is another factor in the manufacture of samples with lower porosity. In addition, a better distribution of grain shape, size and orientation was achieved by Liu et al. [11] through applying a subsequent thermal cycling process. Nevertheless, even setting the optimum process was not possible to achieve a homogenous microstructure over the entire component.

To produce a small laboratory facility for cost effective 3D printing, Gong et al. [12] proposed the fused deposition modelling (FDM) process which is based on an Ultrafuse filament. However, the metal AM parts produced revealed dimensional accuracy issues.

Methods of overcoming the shortcomings of AM (i.e. different level of porosity, inhomogeneous grain sizes and so on) have been studied with a view to enabling AM parts to be used in service. For example, Shao et al. [13] proposed Hot Isostatic Pressing (HIP) as an effective post-process method to reduce porosity. This can reduce the pore radius by at least one to two orders of magnitude. As proved by Blackwell [14] the HIP operation can also significantly reduce anisotropy and eliminate poor interlayer bonding. Wycisk et al. [15] demonstrated that post treatment by HIP is capable of reducing process inherent defects and was able to show a significant improvement in high-cycle fatigue performance as a result. The HIP process is, however, time consuming and costly in terms of materials and equipment.

Abdulhameed et al. [16] indicated a new avenue of using hybrid manufacturing (HM) processes in which different AM methods are combined with subtractive methods or post processing operations. This is intended to overcome the microstructure issues and size limitations posed by AM. A hybrid additive manufacture of 316L stainless steel by combining cold spray and selective laser melting was proposed by Yin et al. [17]. The results were promising, with fully improved mechanical properties being achieved by using a post processing heat treatment. According to Chen et al. [18], the heat processing can only be applied with heat-treatable metallic materials.

To contribute to the development and application of AM at an industrial scale, a hybrid forming technique (AM-micro-forming) was proposed by Jiang et al. [19]. It was further systematically investigated here in order to validate its great potential. This combines the AM approach with hot forging and heat treatment. The proposed method addresses challenges of cost and material. Cost is addressed by the significant reduction in forging operations used in conventional hot forging production as a result of using a near net shape blank, thus reducing tooling and operating costs. For example, this strategy may successfully be applied to reduce the number of forming passes from 5 to only 2 for the manufacture of 316L turbine blades for power station gas turbines, as described in [20]; hence leading to savings in tooling cost. The forging and heat treatment process is aimed at material property aspects, improving the structure of the AM material and avoiding the limitations of ductility and fatigue response associated with current AM metals. This process has also been studied in relation to other materials. Sizova [21] investigated the hot working ability of AM Ti64 (SLM process) with encouraging results. A study into Wire Arc Additive (WAAM) manufactured aluminium alloy AA5083 by Silva [22] was

used to look at formability and void closure in this material when subject to hot compression post-processing.

In addition, the proposed method addresses classical problems such as the significant tool wear encountered when using high performance materials i.e. Titanium (Ti) and Nickel (Ni) alloys. By using the AM approach to produce a preform of the desired geometry enables a reduction in forming operations, reducing material waste and tool changes may lead to increased production throughput. The results gathered in this research enable to confirm the validity of the proposed novel AM-micro-forming procedure. This study also aims to detect the effects produced by the hot forging and heat treatment post processes in respect to the mechanical properties of AM samples. The in-depth mechanisms generated throughout these post-processes route was examined by applying advanced microscopical characterization (EBSD) to observe the grain mechanism and optical observation to detect the porosity evolution during the manufacturing process.

2. Materials and Method

2.1 Sample preparation and processing conditions

Two sets of samples made of AM single phase stainless steel were produced under a Renishaw AM250 Selective Laser Melting Machine. This uses a pulsed laser to fuse the metal powder, with the length of pulse controlling the heat input at any point. Detail of the print parameters are given in Table 1. The print speed was varied by using two different laser exposure pulse times, 88µs and 110µs, thus generating two sample sets of different densities. The shorter exposure time results in a higher laser scan speed and a less dense deposition of material. Table 2 presents particulars of the chemical composition of stainless steel powder used. These AM samples were later submitted to three various post-processing routes to understand and detect a suitable post-processing routine that results in enhancements of the mechanical behaviour. Figure 1 shows a brief schematic of the routine and testing program. The post-processed samples were mechanically machined into their final geometry for tensile testing in agreement with the British Standard (BS) standard [23].

Table 1 Additive Manufacture - Parameters

Power (W)	Spot diameter (µm)	Point distance (µm)	Exposure time (µs)	Hatch spacing (µm)	Layer thickness (µm)	Scan strategy
200	65	60	88 / 110	110	50	bidirectional with 67° rotation between layers

Table 2 Details of chemical composition of AM 316L powder

Elements	**Fe**	**Cr**	**Ni**	**Mo**	**Mn**	**Si**	**N**	**O**	**P**	**C**	**S**
Mass (%)	Balance	16-18	10-14	2-3	≤ 2	≤ 1	≤ 0.1	≤ 0.1	≤ 0.045	≤ 0.03	≤ 0.03

Each set of AM samples contained at least three trials to prove the repeatability of the process, while three batches were used for the different processing stages. Here the first batch of AM samples (Figure 1, yellow route), was examined and tested without incorporating any post processing. Then, the second batch of AM samples was subject to heat treatment only and was sub-divided into two groups for heat treatment at either 900°C or 1040°C for 30 minutes followed by air-cooling (Figure 1, green route). The final batch of AM samples was subjected to hot forging (at either 900°C or 1040°C), applying a displacement rate of 10mm/s. These later samples were then subjected to the same heat treatment applied on the second batch (Figure 1, black route). The processing temperatures were selected based on the lower end of the range recommended for use with commercial processes [24]. During the forging

routine the samples were forged between two flat anvil disks and a witness plate was used to control the amount of deformation.

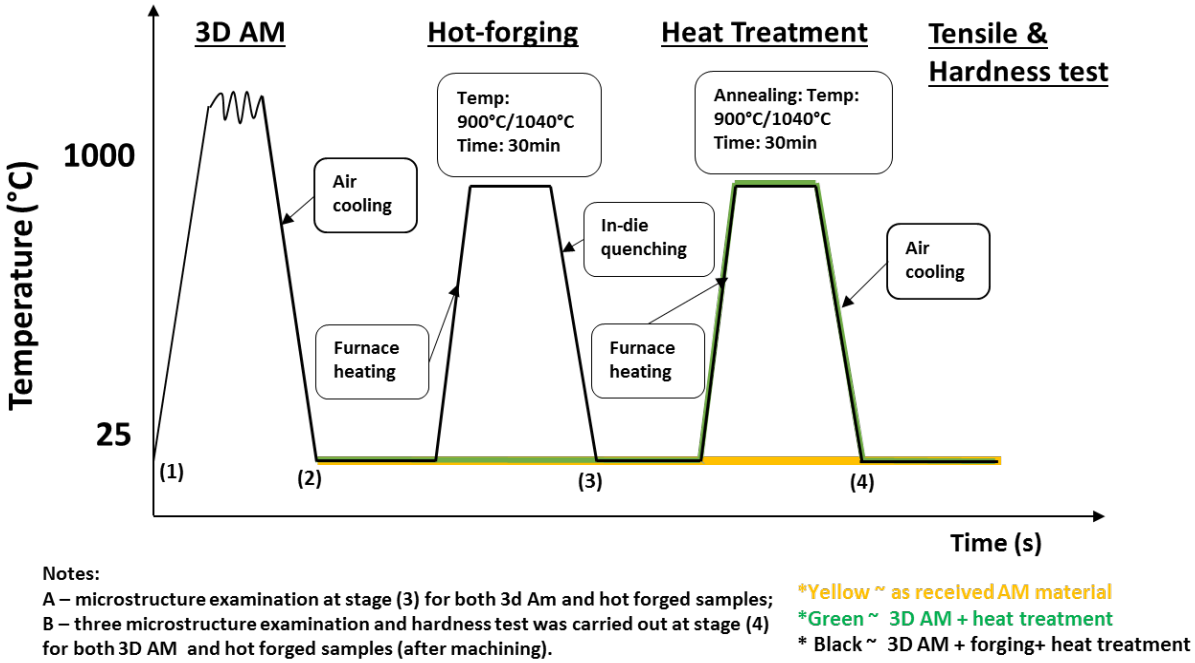

Figure 1 Diagram of material processing for an AM sample submitted to three various post-processes routines. These main processing routes are highlighted as black, green and yellow lines in the figure.

2.2 Hot forging process

A test to replicate conventional hot forging was applied to understand the influence of mechanical deformation on the material properties. To simulate the forging process, a classical Instron hydraulic test machine was used. The forming setup is shown in Figure 2, illustrating the furnace and forming rig, including upper and lower die with preheated facilities. Mechanical loading was applied at a constant displacement rate of 10mm/s, resulting in an effective strain rate of $2sec^{-1}$. Initial die temperature was 20°C. Manual handling was used to transfer the samples from furnace to die. After deformation the samples were held in the die for 10 seconds before being air cooled. This hold time was used to ensure that, as far as possible all samples underwent a consistent thermal process and were not unduly influenced by differences which may have arisen during manually extracting hot samples from the die.

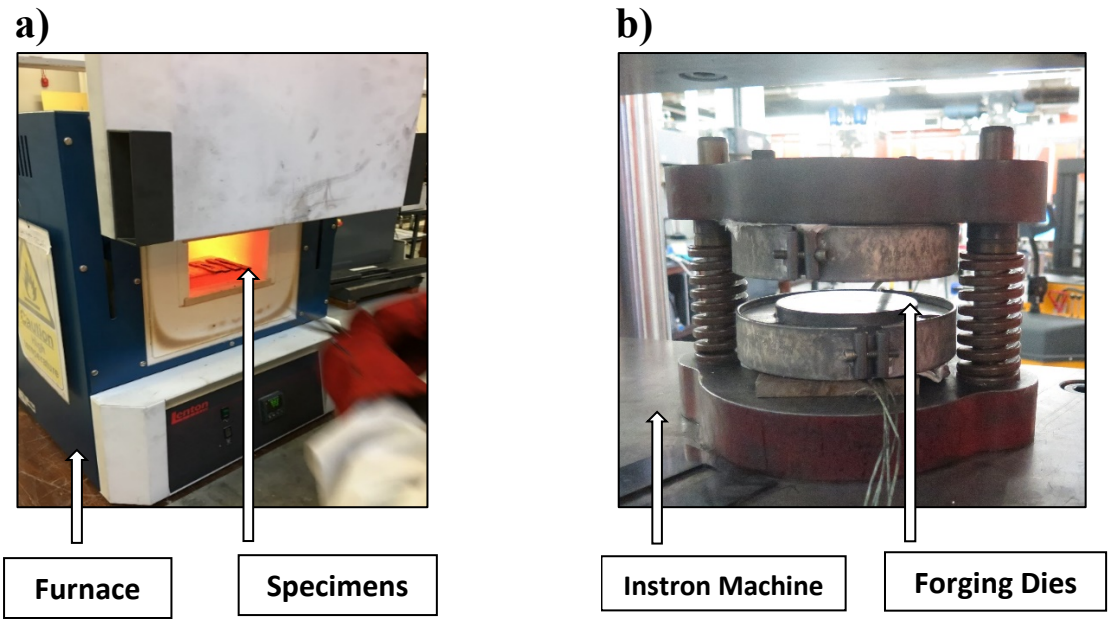

Figure 2 The set-up of the hot forging process. a) Furnace and sample and b) die set u

2.3 Mechanical characterization of AM samples

The mechanical properties were evaluated for hardness and tensile performance. Here, the mechanical hardness tests were conducted on the finish-machined samples in advance of any tensile testing. The mechanical hardness tests were carried out under a Zwick 1875 Vickers hardness apparatus in which were settled a HV10 load.

Tensile tests were conducted by applying a constant displacement rate (0.5mm/min) under an Instron machine, recording load and elongation. The strain was evaluated by using Digital Image Correlation technique in which were recorded the deformation history by tracking the applied speckle pattern.

2.4 Microstructure analysis of samples

The microstructure and porosity of the samples was examined using polished sections taken from the samples. Optical micrographs were used in the evaluation of porosity, and for microstructure studies a scanning electron microscope (SEM) with electron backscatter diffraction (EBSD) capability was used, allowing texture and grain structure to be examined.

The end tabs of the samples were considered for microstructural analysis. These samples were grounded using progressively finer silicon paper (e.g. 800 grit to 4000 grit). The samples were further polished for five minutes using 1 micron diamond suspension and then for a further twenty minutes using colloidal silica polishing. This process allows achieving a mirror surface finish and no induced deformation.

The porosity data were captured using an optical microscope (OM) trademark Zeiss Axio Lab. A Hitachi 3400 SEM incorporating an e flash electron backscatter diffraction (EBSD) electron microscope from Bruker was used to evaluate the microstructure porosity and grain distribution and texture.

3. Results

3.1 Tensile test results

Figure 3 shows the AM sample evolution through the treatment processes. In this figure is clear that the AM samples underwent dimensional change in each process stage. Figure 3(a) shows a sample in the

as received AM condition, presenting a relatively rough surface. Figure 3(b) illustrates the geometry change introduced by the hot forging process. The machined tensile sample with Digital Image Correlation (DIC) speckle coating is shown before and after testing in Figure 3 (c) and (d).

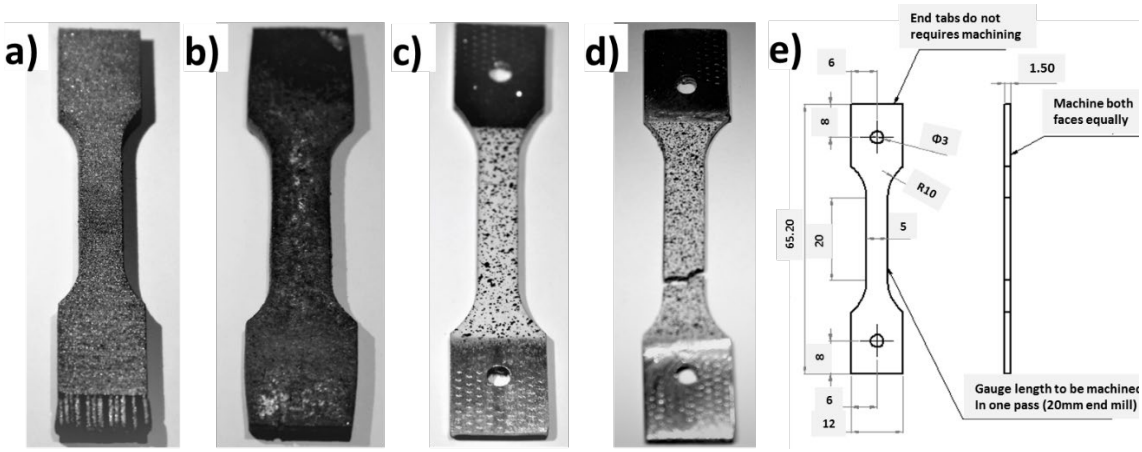

Figure 3 Geometry and dimensions of test pieces at different stages of the investigation processes. (a) AM test piece; (b) hot forged test piece; (c) machined test piece; (d) fractured after mechanical testing; (e) Test Specimen Dimensions.

All prepared samples were subjected to standard tensile tests. Figure 3(e) indicates the nominal specimen dimensions. Figure 4 presents the equivalent true stress-strain curves. The AM samples in their 'as received' condition have poor tensile performance, and this is especially associated with the set manufactured using a higher deposition speed (short exposure pulse) (see Figure 4). The performance of as received AM in the tensile test is about 200MPa. Porosity throughout the bulk of material can be an explanation of poor performance. It was also noted that the ductility was low, at around 2% for the high deposition speed samples. The AM samples in the as received form presented little evidence of any work hardening processes. The AM samples with low speed of deposition (long exposure pulse) (Figure 4b) show better tensile properties. Their yield stress is around 330 MPa while the elongation tends towards 6%. When was analysed the data obtained from samples produced using fast and slow printing, the fast samples showed lower strength and ductility than that one produced by slow printing. The low-strain response (see Figure 4) of the stress-strain curve in the non-linear yielding region may be associated to the formation and propagation of two Lüders bands, which generally nucleate at the ends of the gauge length and further propagate until they meet in the centre of the sample as shown by Luecke and Slotwinski [25].

A massive enhancement on the mechanical properties were obtained by combining the hot forging post process. On the fast-printed samples was obtained an increased tensile strength and ductility more than 200%. Thus, for the high speed of deposition, the yield stress reaches 360 MPa and an elongation of 7%. Moreover, when analysing the slow-printed samples it is noted that the strength increases by almost 50% and ductility increases by 20%. The AM samples processed at the lower scan speed generated the yield stress of 460MPa and an elongation of around 8%.

Figure 4 (a) and 4 (b) reveals that the heat treatment process made only a small improvement for the fast print speed samples and a considerable improvement to the mechanical properties of the slow-printed samples. This might be explained by the accelerated thermal diffusion bonding process which enabled an increase in the microstructure homogeneity, especially for areas of incompletely fused material powder. In addition, as noted in the Figure 4(b), although the tensile strength value of slowly printed samples subjected to heat treatment dropped approximately 30%, its ductility rose dramatically by about 200%.

Major differences in the mechanical properties between as received AM and post processed samples of AM are attributed to the porosity defects (in quantitative and qualitative manner) and grain

morphology. The dislocation density hardening mechanisms in heat treated only samples do not have the significant effects as they do in the hot forged samples where the combination of plastic deformation and subsequent heat treatment may enable a considerable reduction in the total dislocation density.

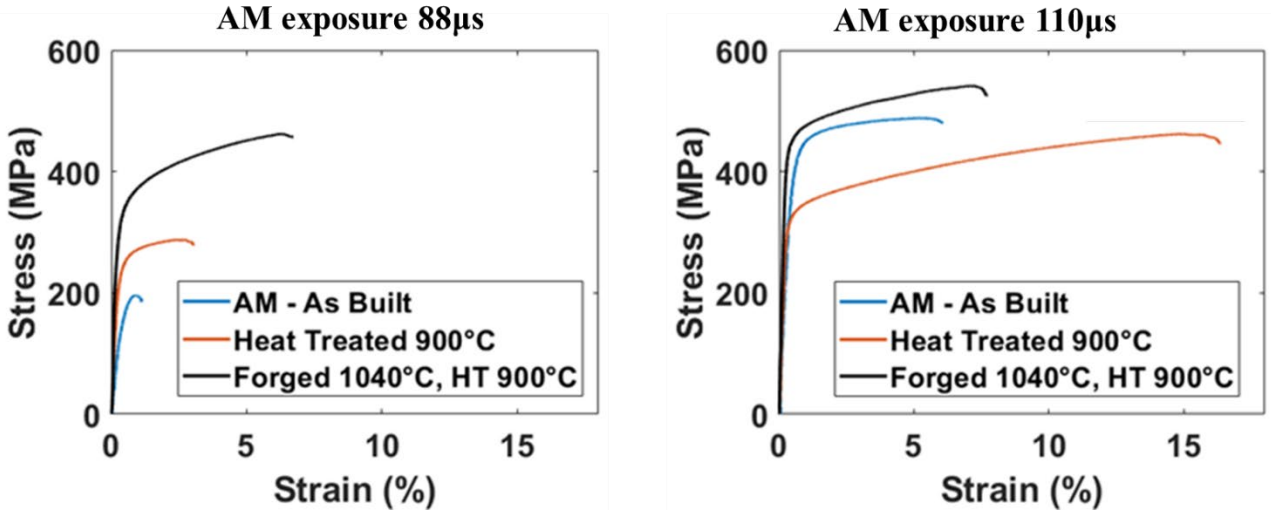

Figure 4 True stress strain curves obtained from AM samples, AM + heat treatment and AM + hot forging and heat treatment with two different printing speeds.

3.2 Hardness tests results

This section highlights the role of metallurgical defects on the mechanical properties (i.e. hardness and the stress/strain response). The hardness tests results presented show the variation of hardness with post-processing and deposition speed. The averaged hardness measurement for different printing speeds from each sample is plotted in Figure 5(a). The slow-printed samples show superior hardness when compared to the fast-printed ones. The numerical value for fast-printed samples range from ~150 HV10 for the as received samples to ~240HV10 for those post processed by hot forming and heating. On the other side, for slow-printed samples in the as received AM form, the numerical values range from 230HV10 to 207HV10. The material may become hardened by applying post heat treatment combined with the hot forging process. Furthermore, the results indicate that the forged and subsequently heat-treated samples reach the highest hardness value. It is approximately 50% higher than that of samples heat-treated alone. Overall, the standard deviation is narrow, showing a good reproducibility on these samples.

The temperature of forging has a limited effect on the hardness, but overall gives an increase in hardness. The hardness of slow-printed samples decreased slightly with heat treatment yet a dramatical increase was seen after applying the hot forging process. This trend also can be seen in proof stress result in Figure 5(b). Merklein et al. [26] showed that the heat treatment can generate increased yield strength due to precipitation hardening. Additional factors contributing to yield strength are dislocation annihilation and recovery occurrence as indicated in [27]. The slow-printed samples have better proof stress than fast-printed ones. Even so, the fast-printed samples show improved properties after the hot forging process and post heat-treatment. Slow-printed samples show similar results to the fast-printed ones, Figure 5(b).

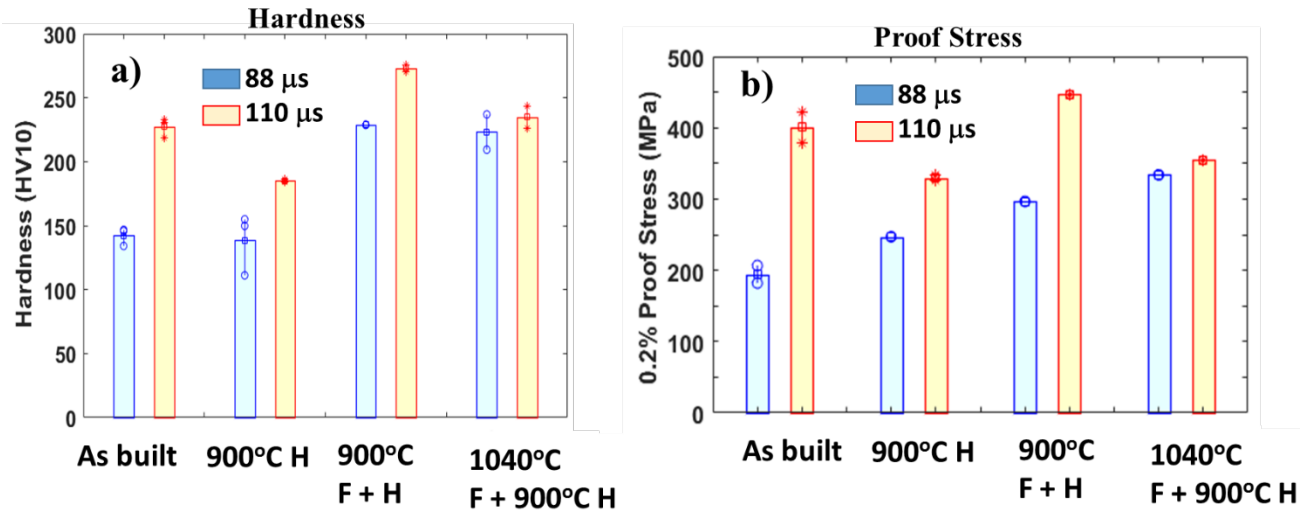

Figure 5 Comparison of mechanical properties of the materials processed at different conditions, namely, direct AM, 900°C heat treatment after printing, 900°C forging and 900°C heat treatment after printing, and 1040°C forging and 900°C heat treatment.

Gong et al. [28] indicated that the defects in AM materials associated to insufficient energy input may have a direct impact on the tensile curve when the porosity exceed 1%. However, the mechanical properties including ultimate tensile strength, elongation values and Young's modulus may deteriorate considerable once the porosity reaches 5% [29].

3.3 UTS and strain at maximum stress

Figure 6 plots the tensile tests results and shows both maximum stress and strain achieved. The results confirm that the forging and heat treatment generate an improvement in the strength for both fast and slow printed samples. The higher forging temperature also gave a stronger performance. The tests performed on as-received samples indicate a maximum stress around ~200MPa for fast deposition and around 450MPa for slow speed of printing. Once the materials were post processed by forging and heating, they reached around 460MPa for fast printing and around 500MPa for slow-printed samples, respectively (Figure 6a). The strain performance also improved following both forging and heat treatments. The maximum strain achieved in as-received samples varies from 2.5% in fast printing to 4% in slow printing, while for the post-processed samples the maximum strain reaches 9% for fast printing and 15% for slow printing respectively (Figure 6b). Here, the heat treated slow-printed sample achieve an elongation between that of the forged samples. This may indicate that even these samples had some initial void content, and by applying the heat treatment, these were reduced by grain growth mechanisms, finally enabling an improvement in tensile performance. Some variation in elongation was noted in the slow-printed samples after 1040°C forging and heat treatment. This may be a result of the manual handling and thermal management of the samples being more critical at the higher temperature.

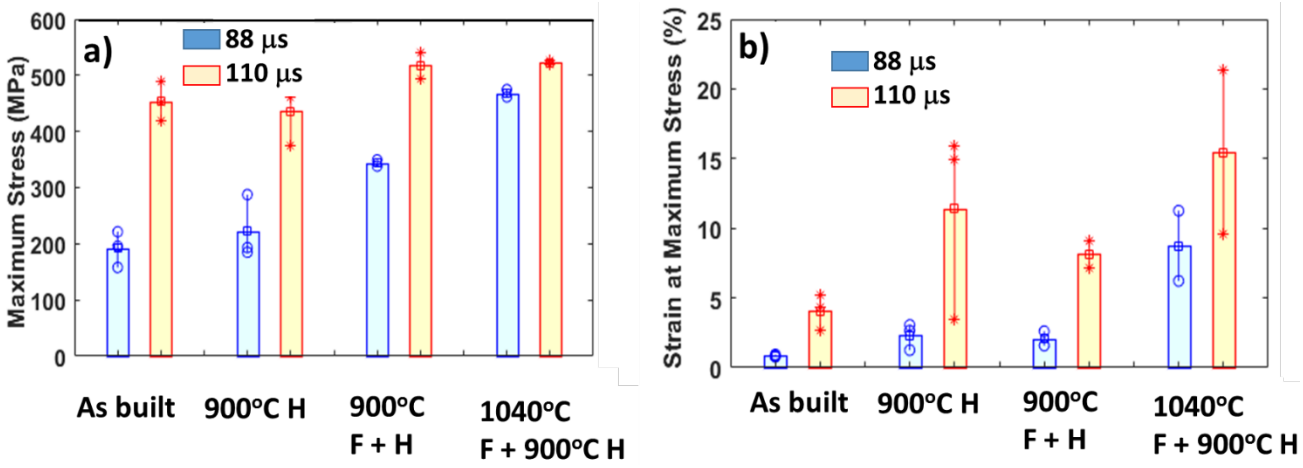

Figure 6 Maximum stress and strain at maximum stress of high speed (blue) and medium speed (yellow) AM samples subjected to various treatments, namely direct AM, 900°C heat treatment after printing, 900°C forging and 900°C heat treatment after printing, and 1040°C Forging and 900°C treatment.

3.4 Microstructure characterization

3.4.1 Porosity-measurements

Quality of AM samples depends on the amount of porosity as well as microstructure. Optical micrographs were used to provide a detailed distribution of porosity generated at each stage during the processing. Figure 7(a) shows the optical micrographs. Further, Figure 7(b) presents their corresponding porosity area fraction in respect to different processing conditions. The higher printing speed generates in areas of higher porosity as compared to slow-printed samples. In the as-received form the material printed at higher speed contains ~4% porosity. Once the samples were heat treated, the porosity amount reached ~11%. After the forging stage the amount of porosity was reduced to ~1.5%. By evaluation the fast-printed samples, we recognised that the heat treatment process can close or reduce small voids, whereas the hot forging process is a much more effective tool to decrease the size and population of voids. The higher temperature of forging could also result in the improvement of tensile properties. However, the slow-printed samples have lower initial porosity, consequently the combined hot forging and heat treatment processes may had limited scope for the reduction of voids. On the slow printing speed, the amount of porosity varies from ~1.5% on as received samples to 0.5 % on the heated and forged samples.

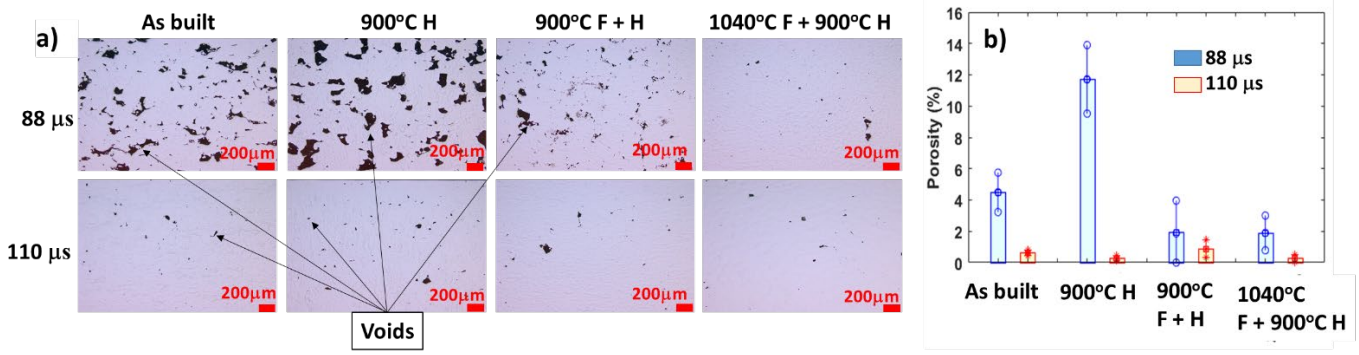

Figure 7 Porosity variations when material is processed through different conditions for 2 different AM speeds. a) qualitative measurement using optical evaluation and b) quantitative percentage of porosity in samples analysed.

As per literature recommendation, the high scanning speeds should be correlated to high laser power while using short hatch distances to obtain superior samples. Otherwise, as Meier et al. [30] showed, the production of a dense non-porous material is not possible.

3.4.2 Crystal orientation characterisation

Crystal orientation characterisation and grain size analysis are useful tools in explaining why properties of samples change after heat treatment and hot forging. The electron backscatter diffraction (EBSD) technique is designed to provide just such analytical data, and is one of the best ways of determining the microstructure and characterisation of samples. The quality of the EBSD microstructural image is highly dependent on the sample surface quality. To avoid any issue when preparing stainless steel samples in terms of quality, the surface preparation was checked by optical microscope before performing EBSD.

A detailed crystallography orientation characterisation was performed on these samples. This enabled the grain size distribution and their evolution to be detected. Figure 8 shown the EBSD images after noise reduction. The bar plot, Figure 9(a) gives average grain size. Slowly printed samples are bounded by smaller grain size compared to fast-printed ones for the same condition. For both sets, however, grains are greatly refined after the hot forging and heat treatment process. It is observed that the average grain size has comparable values in both cases, as seen in Figure 9(a). The forming method for the AM samples may result in high dislocation densities, potentially driven by the severe thermal stress generated by the localised heat input of the scanning laser. Accordingly to Sun et al. [31] these dislocations may be reduced during the heat treatment processes. The hot forging could, however, result in increased dislocations resulted from the deformation input. In heat treatment, the occurance of recrystallization, Figure 9(b), is explained through the formation of refined grains. A higher temperature appears to increase this recrystallization process and form finer grain sizes. The EBSD results help to explain the evolution mechanisms during the hot forging and heat treatment which help to enhance the mechanical properties of the AM samples. The refined grain size occurred during SLM metals may help to increase the strength of materials when compared to wrought equivalents. However, we consider that a far more important contribution is that generated by the high dislocation densities present in the as-built structures after SLM. These will spread homogeneously as heat treatment and forging are applied, as according to Gorsse et al. [32]. The initial texture observed in AM material parts can be associated to thermal gradients. This can be more accentuated around the melt pool during solidification, observations which agree with [33]. The changes in texture generated by the additional heat treatment and forging process mechanisms may further enable modification of the microstructure composition.

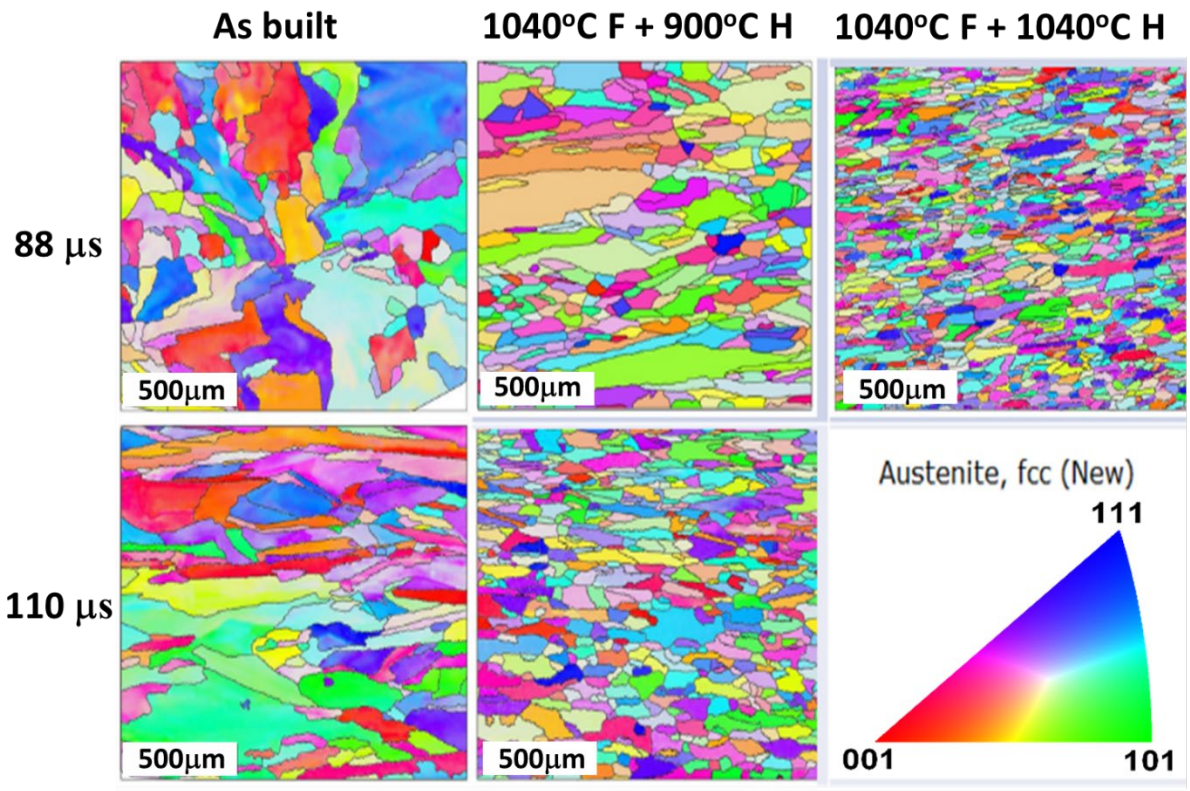

Figure 8 Comparison of crystal orientation characterization and grain size variations of the material processed at different conditions for the two AM speeds using a qualitative measurement with the EBSD technique.

Recrystallization is an important index parameter to account for the grain growth process. In this analysis, the microstructure recrystallized fraction was quantified by considering the average recrystallized grain size (RGS). However, Victoria-Hernandez et al. [34] found difficulty in separating the effect of recrystallized basal grain growth, which helps to reduce the stored strain of neighbouring grains, from the one produced by the effect of grain growth enabling a decrease in grain boundary area. The later one can helps to reduce the internal stored energy. The recrystallization fraction determined from the smoothed EBSD maps is shown in Figure 9(b). Both fast and slow printed samples in the same condition have similar percentages of recrystallization. The hot forging process provides an improvement in recrystallization quantity. The heat treatment process alone, however, had only a limited effect on the recrystallization process. The temperature of the hot forging process is also shown to affect recrystallization, this being increased at the higher forging temperature. The refinement process of grain size may be responsible for the mechanical response (and anisotropy). Herzog et al. [35] and Lewandowski and Seifi [36] revealed that a reduction in grain size from 30-50 µm to about 10 µm will cause an increase in Hall–Petch strengthening for this material. The formation of columnar together with epitaxial growth and some elongated grains was also observed. The tendency of elongated grains formation may extend over multiple AM build layers and the grain structure generally may be strongly dependent on local boundary conditions such as component geometry and scan pattern. Accordingly to Gunther et al. [37] these factors may introduce local variations in the cooling rate which can affect the solidification process.

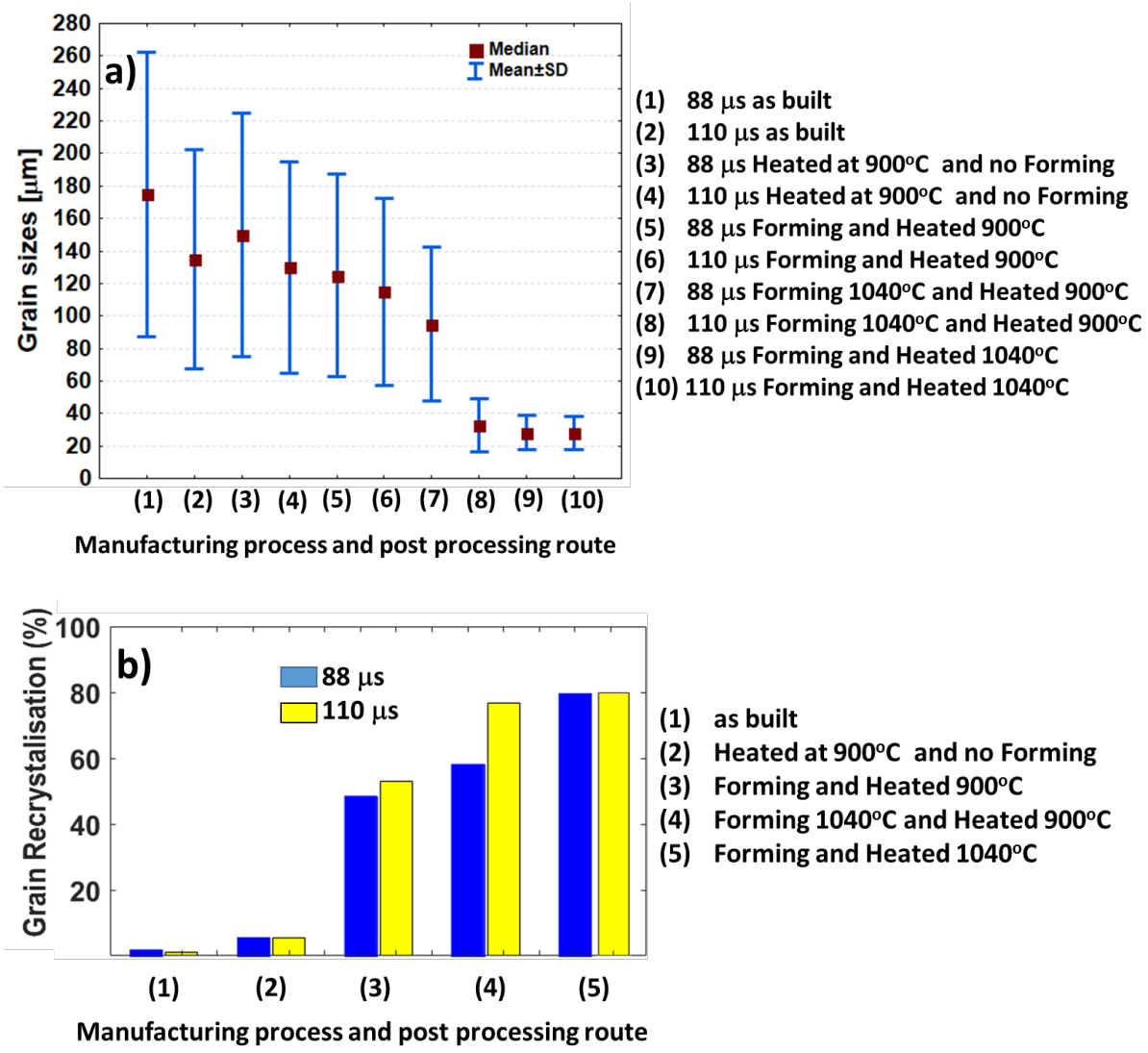

Figure 9 Quantitative distribution of grain in the samples analysed and b) Grain recrystallization percentage of fast speed (blue) and slow speed (yellow) AM samples subjected to five various treatments, namely direct AM, 900°C heat treatment after printing, 900°C forming and heat treatment, 1040°C forming and 900°C heat treatment, and 1040°C forming and treatment.

When the printed samples reach 100% consolidation through increased energy input, softening effects may result from grain growth reducing the grain boundary volume fraction, therefore the hardening effects of dislocation pinning may be reduced.

4. Discussion

Significant amounts of porosity may be realised during the AM building process for a variety of reasons. Accordingly to Reijonen et al. [38] the most influential operating factors are the parameters of the AM machine itself, (power, speed, accuracy), the build parameters (scan pattern, component size, build step, and the qualities of the feed material used (purity, particle size, consistency). These porosity defects are presented as a mix of larger and smaller defects. Commonly larger irregular pores may be associated to lack of melting or/and shrinkage micropores which are dictated by the lack of material feed within inter-dendritic zones, and spherical pores are due to the presence of trapped gasses in the feedstock material, as per Henaff et al. [39].

The larger defects are more dependent on the build parameters, resulting in areas of incomplete fusion or regions where the material flow has created voids. Higher laser scan speeds can generate a longer melt pool, therefore is induced a much-extended melt surface area. Further, when the vaporisation and the temperature gradient surrounding the melt pool is more accentuated, an increase on the Marangoni force occur and the melt flow instability are produced as per Qiu et al. [40]. Further, Iebba et al. [41] showed that an inadequate heat transfer applied on the powder bed may also cause unstable melt flow which can be responsible for increased porosity and surface roughness.

Smaller porosity defects may result from entrapment of the inert shielding gas. A major source of gas pores can be attributed to powder feedstock, where argon may be been trapped in the powder particles during the plasma atomisation manufacturing process. However, Reijonen et al. [38] attributed the source to be from the shielding gas used in the AM build process.

The presence of irregular pores geometry accumulated during AM builds are very dangerous because it produces an accumulation of high stress concentrations and can thus generate lower failure strain and strength values, see for example Figure 6. The literature confirms that porosity defects lead to a decrease in mechanical properties [42]. By introducing the hot forging and heat treatment strategy described here, the failure strain values increased by a factor of three, and stress resistance doubled in the post-processed samples compared to the as-built samples.

Other considerations which help to understand the benefits of the post-processing strategy are shown by differences in the amount of porosity which occur at different deposition speeds. It was demonstrated that a higher deposition speed would generate a larger degree of porosity when compared with the lower speed of deposition (Figure 7(a)). The combined heat treatment and forging deformation facilitates the reduction in porosity to near 1%, Figure 7(b).

Once the amount of porosity was reduced, it was possible to obtain a constant level of hardness for both speeds of deposition (88 and 110μs) as shown in Figure 5(a). This indicated that the post process was successful in eliminating the effects of the different initial porosity levels.

Zhang et al. [43] indicated that an appropriate treatment, i.e. heat treatment, enables enhanced AM sample tensile strength by generating precipitation hardening which is the key to high strength and hardness. The quenching rates generated by the conduction of heat over the substrate during build are sufficiently fast to create a quick solidification microstructure. Gu et al. [44] noted that grain refinement may occur and generate stronger performance in AM processed materials. From our study, it was observed that heat treatment could make the microstructure homogeneous in the AM samples, resulting in major improvement of the mechanical properties. To eliminate the in-homogeneity of the microstructure (in as-printed samples) and reduce the porosity, samples were subjected to different heat treatment and forming strategies. During this combined process the particle grains connect with each other and are distributed evenly in the matrix. The average grain sizes reduce from around 140-180μm in as-built state to around 25μm when post processed (see Figure 8 for details).

The high amount of recrystallization that occurred in our process could be due to competition between the plastic strains imposed during forging and the change in the thermal gradient as a result of the in-die cooling after forging. The results show that the greatest grain recrystallization was generated at the higher forging and heat treatment temperatures and resulted in finer grains.

5. Conclusions

In this paper, a new method combining AM with the hot forging and heat treatment process is presented as a way of enhancing the mechanical properties of AM material. In this study the proposed method is investigated through tensile and hardness tests, as well as optical observation and EBSD microstructure characterization of AM 316L Stainless Steel samples produced under different build conditions. The following conclusions can be indicated:

1. The AM samples printed with a longer laser exposure time exhibited higher mechanical performance compared to short exposure samples and contained less porosity.
2. Hot Forging the AM samples dramatically reduced porosity in the material.
3. The hot forging process provided a dramatic improvement in the mechanical properties of AM samples. In addition, the EBSD maps obtained during this process indicated a refinement of grain size and an increase in the recrystallization process.
4. Combining hot forging with the heat treatment process offers a greater improvement in mechanical properties when compared with the heat treatment process alone.

Acknowledgements

The financial support from the First Aircraft Institute (FAI) of Aviation Industry Corporation of China (AVIC) Ltd is kindly acknowledged by C. Hopper and Z. Tan. The research was performed at the AVIC Centre for Structural Design and Manufacture at Imperial College London.

Compliance with ethical standards

Conflict of interest: The authors declare that they have no conflict of interest.

References

[1] W.E. Frazier, Metal Additive Manufacturing: A Review, Journal of Materials Engineering and Performance 23(6) (2014) 1917-1928.
[2] J.P. Kruth, M.C. Leu, T. Nakagawa, Progress in Additive Manufacturing and Rapid Prototyping, CIRP Annals 47(2) (1998) 525-540.
[3] L.E. Murr, S.M. Gaytan, F. Medina, H. Lopez, E. Martinez, B.I. Machado, D.H. Hernandez, L. Martinez, M.I. Lopez, R.B. Wicker, J. Bracke, Next-generation biomedical implants using additive manufacturing of complex, cellular and functional mesh arrays, Philos Trans A Math Phys Eng Sci 368(1917) (2010) 1999-2032.
[4] S. Ghouse, S. Babu, R.J. Van Arkel, K. Nai, P.A. Hooper, J.R.T. Jeffers, The influence of laser parameters and scanning strategies on the mechanical properties of a stochastic porous material, Materials & Design 131 (2017) 498-508.
[5] H. Lee, C.H.J. Lim, M.J. Low, N. Tham, V.M. Murukeshan, Y.-J. Kim, Lasers in additive manufacturing: A review, International Journal of Precision Engineering and Manufacturing-Green Technology 4(3) (2017) 307-322.
[6] X. Wang, D. Deng, M. Qi, H. Zhang, Influences of deposition strategies and oblique angle on properties of AISI316L stainless steel oblique thin-walled part by direct laser fabrication, Optics & Laser Technology 80 (2016) 138-144.
[7] M. Pellizzari, B. AlMangour, M. Benedetti, S. Furlani, D. Grzesiak, F. Deirmina, Effects of building direction and defect sensitivity on the fatigue behavior of additively manufactured H13 tool steel, Theoretical and Applied Fracture Mechanics (2020) 102634.
[8] P. Karimi, T. Raza, J. Andersson, L.E. Svensson, Influence of laser exposure time and point distance on 75-µm-thick layer of selective laser melted Alloy 718, The International Journal of Advanced Manufacturing Technology 94(5-8) (2017) 2199-2207.
[9] J.A. Cherry, H.M. Davies, S. Mehmood, N.P. Lavery, S.G.R. Brown, J. Sienz, Investigation into the effect of process parameters on microstructural and physical properties of 316L stainless steel parts by selective laser melting, The International Journal of Advanced Manufacturing Technology 76(5) (2015) 869-879.

[10] J.P.M. Pragana, P. Pombinha, V.R. Duarte, T.A. Rodrigues, J.P. Oliveira, I.M.F. Bragança, T.G. Santos, R.M. Miranda, L. Coutinho, C.M.A. Silva, Influence of processing parameters on the density of 316L stainless steel parts manufactured through laser powder bed fusion, Proceedings of the Institution of Mechanical Engineers, Part B: Journal of Engineering Manufacture (2020) 0954405420911768.
[11] Y. Liu, Z. Pang, J. Zhang, Comparative study on the influence of subsequent thermal cycling on microstructure and mechanical properties of selective laser melted 316L stainless steel, Applied Physics A 123(11) (2017) 688.
[12] H. Gong, D. Snelling, K. Kardel, A. Carrano, Comparison of Stainless Steel 316L Parts Made by FDM- and SLM-Based Additive Manufacturing Processes, JOM 71(3) (2019) 880-885.
[13] S. Shao, M.J. Mahtabi, N. Shamsaei, S.M. Thompson, Solubility of argon in laser additive manufactured α-titanium under hot isostatic pressing condition, Computational Materials Science 131 (2017) 209-219.
[14] P.L. Blackwell, The mechanical and microstructural characteristics of laser-deposited IN718, Journal of Materials Processing Technology 170(1) (2005) 240-246.
[15] E. Wycisk, S. Siddique, D. Herzog, F. Walther, C. Emmelmann, Fatigue Performance of Laser Additive Manufactured Ti–6Al–4V in Very High Cycle Fatigue Regime up to 109 Cycles, Frontiers in Materials 2 (2015).
[16] O. Abdulhameed, A. Al-Ahmari, W. Ameen, S.H. Mian, Additive manufacturing: Challenges, trends, and applications, Advances in Mechanical Engineering 11(2) (2019) 1687814018822880.
[17] S. Yin, X. Yan, R. Jenkins, C. Chen, M. Kazasidis, M. Liu, M. Kuang, R. Lupoi, Hybrid additive manufacture of 316L stainless steel with cold spray and selective laser melting: Microstructure and mechanical properties, Journal of Materials Processing Technology 273 (2019) 116248.
[18] N. Chen, G. Ma, W. Zhu, A. Godfrey, Z. Shen, G. Wu, X. Huang, Enhancement of an additive-manufactured austenitic stainless steel by post-manufacture heat-treatment, Materials Science and Engineering: A 759 (2019) 65-69.
[19] J. Jiang, P. Hooper, N. Li, Q. Luan, C. Hopper, M. Ganapathy, J. Lin, An integrated method for net-shape manufacturing components combining 3D additive manufacturing and compressive forming processes, Procedia Engineering 207 (2017) 1182-1187.
[20] H. Kohei, O. Hiroharu, M. Yasuo, U. Naoyuki, K. Shuhei, H. Hidetaka, M. Takumi, Turbine blade manufacturing method, in: U. A1 (Ed.) 2016.
[21] I. Sizova, M. Bambach, Hot workability and microstructure evolution of pre-forms for forgings produced by additive manufacturing, Journal of Materials Processing Technology 256 (2018) 154-159.
[22] C.M.A. Silva, I.M.F. Bragança, A. Cabrita, L. Quintino, P.A.F. Martins, Formability of a wire arc deposited aluminium alloy, Journal of the Brazilian Society of Mechanical Sciences and Engineering 39(10) (2017) 4059-4068.
[23] BSI, BS EN ISO 6892-1:2016, Metallic materials — Tensile testing, BSI Standards Limited 2016.
[24] Aalco, Stainless Steel 14401 316 Sheet and Plate Quarto Plate CPP Plate 345, in: Aalco_Metals_Ltd (Ed.) 2020.
[25] W.E. Luecke, J.A. Slotwinski, Mechanical Properties of Austenitic Stainless Steel Made by Additive Manufacturing, J Res Natl Inst Stand Technol 119 (2014) 398-418.
[26] M. Merklein., R. Plettke., D. Junker., A. Schaub., B. Ahuja., "Mechanical Testing of Additive Manufactured Metal Parts", Key Engineering Materials Vols. 651-653, (2015) pp. 713-718.
[27] O. Renk, A. Hohenwarter, K. Eder, K.S. Kormout, J.M. Cairney, R. Pippan, Increasing the strength of nanocrystalline steels by annealing: Is segregation necessary?, Scripta Materialia 95 (2015) 27-30.
[28] H. Gong, K. Rafi, H. Gu, G.D. Janaki Ram, T. Starr, B. Stucker, Influence of defects on mechanical properties of Ti–6Al–4V components produced by selective laser melting and electron beam melting, Materials & Design 86 (2015) 545-554.
[29] S. Gorsse, C. Hutchinson, M. Goune, R. Banerjee, Additive manufacturing of metals: a brief review of the characteristic microstructures and properties of steels, Ti-6Al-4V and high-entropy alloys, Sci Technol Adv Mater 18(1) (2017) 584-610.

[30] H. Meier, C. Haberland, Experimental studies on selective laser melting of metallic parts, Materialwissenschaft und Werkstofftechnik 39(9) (2008) 665-670.
[31] Z. Sun, X. Tan, S.B. Tor, W.Y. Yeong, Selective laser melting of stainless steel 316L with low porosity and high build rates, Materials & Design 104 (2016) 197-204.
[32] S. Gorsse, C. Hutchinson, M. Gouné, R. Banerjee, Additive manufacturing of metals: a brief review of the characteristic microstructures and properties of steels, Ti-6Al-4V and high-entropy alloys, Sci Technol Adv Mater. 18(1): 584–610, 2017.
[33] P.C. Collins, D.A. Brice, P. Samimi, I. Ghamarian, H.L. Fraser, Microstructural Control of Additively Manufactured Metallic Materials, Annual Review of Materials Research 46(1) (2016) 63-91.
[34] J. Victoria-Hernandez, S. Yi, J. Bohlen, G. Kurz, D. Letzig, The influence of the recrystallization mechanisms and grain growth on the texture of a hot rolled AZ31 sheet during subsequent isochronal annealing, Journal of Alloys and Compounds 616 (2014) 189-197.
[35] D. Herzog, V. Seyda, E. Wycisk, C. Emmelmann, Additive manufacturing of metals, Acta Materialia 117 (2016) 371-392.
[36] J.J. Lewandowski, M. Seifi, Metal Additive Manufacturing: A Review of Mechanical Properties, Annual Review of Materials Research 46(1) (2016) 151-186.
[37] J. Günther, F. Brenne, M. Droste, M. Wendler, O. Volkova, H. Biermann, T. Niendorf, Design of novel materials for additive manufacturing - Isotropic microstructure and high defect tolerance, Scientific Reports 8(1) (2018) 1298.
[38] J. Reijonen, A. Revuelta, T. Riipinen, K. Ruusuvuori, P. Puukko, On the effect of shielding gas flow on porosity and melt pool geometry in laser powder bed fusion additive manufacturing, Additive Manufacturing 32 (2020) 101030.
[39] G. Hénaff, Z. Zhou, X. Hua, C. Li, G. Chen, The effect of texture on the low cycle fatigue property of Inconel 718 by selective laser melting, MATEC Web of Conferences 165 (2018).
[40] C. Qiu, C. Panwisawas, M. Ward, H.C. Basoalto, J.W. Brooks, M.M. Attallah, On the role of melt flow into the surface structure and porosity development during selective laser melting, Acta Materialia 96 (2015) 72-79.
[41] M. Iebba, A. Astarita, D. Mistretta, I. Colonna, M. Liberini, F. Scherillo, C. Pirozzi, R. Borrelli, S. Franchitti, A. Squillace, Influence of Powder Characteristics on Formation of Porosity in Additive Manufacturing of Ti-6Al-4V Components, Journal of Materials Engineering and Performance 26(8) (2017) 4138-4147.
[42] J.K. Tiwari, A. Mandal, N. Sathish, A.K. Agrawal, A.K. Srivastava, Investigation of porosity, microstructure and mechanical properties of additively manufactured graphene reinforced AlSi10Mg composite, Additive Manufacturing 33 (2020) 101095.
[43] M. Zhang, C. Chen, B. Ren, Effect of heat treatment on the microstructure of Co–Cr–W alloy fabricated by laser additive manufacturing, Optical Engineering 57(04) (2018).
[44] D.D. Gu, W. Meiners, K. Wissenbach, R. Poprawe, Laser additive manufacturing of metallic components: materials, processes and mechanisms, International Materials Reviews 57(3) (2013) 133-164.